



Structure-guided 3D anisotropic tomography: a case study

Jessé Carvalho Costa (UFPA), Eduardo Filpo* (PETROBRAS), Luiz Alberto Santos (PETROBRAS) and Etory Feller Sperandio (PETROBRAS)

Copyright 2019, SBGf - Sociedade Brasileira de Geofísica

This paper was prepared for presentation during the 16th International Congress of the Geophysical Society held in Rio de Janeiro, Brazil, 19 to 22 August 2019.

Contents of this paper were reviewed by the Technical Committee of the 16th International Congress of the Brazilian Geophysical Society. Ideas and concepts of the text are authors' responsibility and do not necessarily represent any position of the SBGf, its officers or members. Electronic reproduction or storage of any part of this paper for commercial purposes without the written consent of the Brazilian Geophysical Society is prohibited.

Abstract

Macro-velocity model building remains a challenge for seismic imaging. Currently, seismic datasets with large offsets and multi-azimuth usually require anisotropic models to produce a consistent 3D image of subsurface. The larger number of parameters to represent anisotropic models increases the ambiguity in 3D tomography. We present a successful case study illustrating the importance of using carefully designed conditioning of common image point gathers (CIP), dense RMO events picking and interactive QC tools, combined with 3D anisotropic structure guided tomography in order to reduce ambiguity and estimate a geologically conformable velocity model.

Introduction

Imaging seismic data with large offsets and multi-azimuths accurately demands 3D anisotropic tomography. The methodology for tomography in anisotropic media is well established in the literature (Barbosa et al., 2008; Bakulin et al., 2010; Zhou et al., 2011; Wang and Tsvankin, 2013), however, its implementation is not trivial. A carefully designed 3D tomography workflow still is an important and robust processing tool for 3D seismic imaging. We present a case study where two implementations of tomography produced noticeable differences in the velocity model and the resulting 3D seismic image. The baseline velocity model for our study is VTI and was produced by a service company after five iterations of 3D anisotropic tomography. The interpreter was not satisfied with the results and suggested further investigation for reducing the RMO through isotropic iterations. In order to evaluate the interpreter conjecture we used an in house implementation of 3D anisotropic structure-oriented tomography. The main features of our tomography implementation consist of a raytracing implementation for arbitrary Hamiltonians, model representation using nonuniform B-splines of variable order, structure-guided preconditioning (Hale, 2009) and multi-scale iterations strategy. Also critically important was a robust implementation of dense event picking and interactive QC. Using this approach we validated the interpreter conjecture with a velocity model that reduced the RMO in all CIP compared with the baseline result for the whole offset range. Consequently, the resulted image is better focused. Surprisingly, the isotropic velocity

model, structurally conformable, was more consistent with the dataset than the baseline anisotropic model.

Methodology

The anisotropic 3D tomography follows closely the methodology for raytracing and computation of Frechét derivatives presented by Barbosa et al. (2008). Given an Hamiltonian $\mathcal{H}(\mathbf{x}, \mathbf{p}; \mathbf{C}) = 0$, defined by an eikonal equation for each position \mathbf{x} and slowness vector \mathbf{p} , for a set of material parameters represented by \mathbf{C} . For example, to model qP TTI anisotropy we use the anelliptical approximation (Schoenberg and de Hoop, 2000):

$$\begin{aligned} \mathcal{H}(\mathbf{x}, \mathbf{p}) = & \frac{1}{2} \left[C_\varepsilon(\mathbf{x})(\mathbf{p} \cdot \mathbf{p} - (\mathbf{p} \cdot \mathbf{v}(\mathbf{x}))^2) + C_0(\mathbf{x})(\mathbf{p} \cdot \mathbf{v}(\mathbf{x}))^2 \right. \\ & - C_0(\mathbf{x})(C_\varepsilon(\mathbf{x}) - C_\delta(\mathbf{x}))(\mathbf{p} \cdot \mathbf{p} - (\mathbf{p} \cdot \mathbf{v}(\mathbf{x}))^2)(\mathbf{p} \cdot \mathbf{v}(\mathbf{x}))^2 \\ & \left. - 1 \right] = 0, \end{aligned} \quad (1)$$

where C_0 represents the square of propagation velocity along the symmetry axis, $C_\varepsilon \equiv C_0(1 + 2\varepsilon)$ and $C_\delta \equiv C_0(1 + 2\delta)$; ε and δ are the Thomsen's parameters (Thomsen, 1986); $\mathbf{v}(\mathbf{x})$ indicates the direction of the symmetry axis.

The residual moveout at CIP gathers relative to a reference offset h_0 , i.e., $\delta z_{rmo} \equiv z(h) - z(h_0)$, can be modeled by the fundamental equation of tomography in the migrated domain:

$$\begin{aligned} z(h) - z(h_0) = & - \frac{1}{\|\mathbf{p}^s(h) + \mathbf{p}^r(h)\| \mathbf{n} \cdot \mathbf{e}_z} \\ & \left(\int_0^{T^s(h)} \frac{\partial \mathcal{H}}{\partial \mathbf{C}} \delta \mathbf{C} d\tau + \int_0^{T^r(h)} \frac{\partial \mathcal{H}}{\partial \mathbf{C}} \delta \mathbf{C} d\tau \right) \\ & + \frac{1}{\|\mathbf{p}^s(h_0) + \mathbf{p}^r(h_0)\| \mathbf{n} \cdot \mathbf{e}_z} \\ & \left(\int_0^{T^s(h_0)} \frac{\partial \mathcal{H}}{\partial \mathbf{C}} \delta \mathbf{C} d\tau + \int_0^{T^r(h_0)} \frac{\partial \mathcal{H}}{\partial \mathbf{C}} \delta \mathbf{C} d\tau \right). \end{aligned} \quad (2)$$

Equation (2) determines a linear relationship between the event residual moveout and the perturbations of velocity model parameters $\delta \mathbf{C}$ around a current reference model \mathbf{C} . In order to build a linear system using this equation we need to compute pairs of specular rays from each picked event to the surface constrained to fit the offsets, h and h_0 , and azimuth; \mathbf{p}^s and \mathbf{p}^r are the initial slowness vector at CIP depth for the ray branch to source and to receiver, respectively; T^s and T^r represent traveltimes for each branch from the event coordinates to the surface for a defined offset and azimuth, \mathbf{n} is the direction normal to a possible reflector and, \mathbf{e}_z the vertical direction.

The model parameters are specified using B-splines interpolation (De Boor et al., 1978; Piegl and Tiller, 2012). The value of each parameter at a given position, $C^n(x, y, z)$ for $n \in \{1, \dots, N\}$, is uniquely defined by corresponding

coefficients C_{ijk}^n specified in a 3D control mesh of dimensions $N_x \times N_y \times N_z$, i.e.,

$$C^n(x, y, z) = \sum_i \sum_j \sum_k C_{ijk}^n B_1^i(x) B_2^j(y) B_3^k(z), \quad (3)$$

where $B_1^i(x), B_2^j(y), B_3^k(z)$ represents the B-splines polynomial bases along each coordinate direction. Substituting the representation above in equation (2) produces the linear system which allows us to determine δC_{ijk}^n and update the model. The implementations permits nonuniform meshes and B-Splines of variable order.

The linear system resulting from equation (2) is, in general, poorly conditioned (Woodward et al., 2008; Golub and Van Loan, 2012). In order to assure stable linear iterations it is necessary the introduction of supplementary information about the model properties. A classical approach to stabilization is regularization (Costa et al., 2008). More recently, in order to estimate geologically conformable models, inclusion of structural information to better conditioning geophysical inversion have been and continue being developed (Clapp et al., 2004; Ma et al., 2012; Shank et al., 2017; Li et al., 2018; Zhou et al., 2016; Guo et al., 2017). Our implementation used the structural smoothing equation (Hale, 2009) to enforce a conformable geological model,

$$m(\mathbf{x}) - \frac{1}{2} \nabla \cdot (\alpha(\mathbf{x}) \mathbf{D}(\mathbf{x}) \nabla m(\mathbf{x})) = q(\mathbf{x}), \quad (4)$$

where $m(\mathbf{x})$ represents the update of a model component, $\delta C^n(\mathbf{x})$, and $q(\mathbf{x})$ its reparameterization following Harlan (1995); $\mathbf{D}(\mathbf{x})$ is the diffusivity tensor, i.e., the inverse of the structure tensor (Fehmers and Höcker, 2003), finally $\alpha(\mathbf{x})$ is a normalized coherence and allows for structural discontinuities (Hale, 2009). The numerical solution of equation (4) in a dense grid formally corresponds to a model reparameterization, which can be represented by the matrix operation $\mathbf{m} = \mathbf{P}\mathbf{q}$. The model update requires the least squares solution of the linear system:

$$\begin{pmatrix} \mathbf{LP} \\ \lambda_m \mathbf{I} \end{pmatrix} \mathbf{q} = \begin{pmatrix} \mathbf{d} \\ \mathbf{0} \end{pmatrix}, \quad (5)$$

where \mathbf{L} represents the tomographic matrix associated to equation (2), \mathbf{d} contains selected RMOs and λ_m is a damping parameter. We use the LSMR algorithm (Fong and Saunders, 2011) to solve the linear system in equation (5).

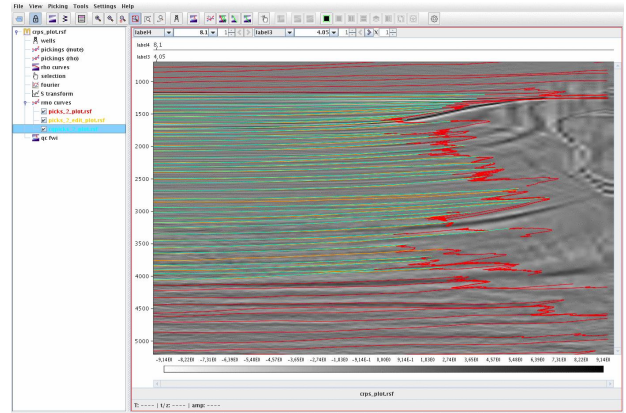


Figure 1: Dense picking of RMO events and interactive QC.

RMO picking and quality control are critical for successful field data applications of seismic tomography. The event selection is performed in three steps: 1) free picking of the largest number of events up to a prescribed number; 2) selection of events with automatic quality control and, 3) fitting of the selected events with a polynomial of variable degree. Figure 1 shows an example of a CIP gather with the curves resulting from the steps in the event selection, the red curves represent the first step in the selection process, orange curves are produced by the automatic quality control, cyan curves correspond to the polynomial fitting of selected events. One can notice that the polynomial fitting also contributes to QC discarding some of the previously selected events.

Figure contains the flowchart of our methodology for structure-guided anisotropic tomography.

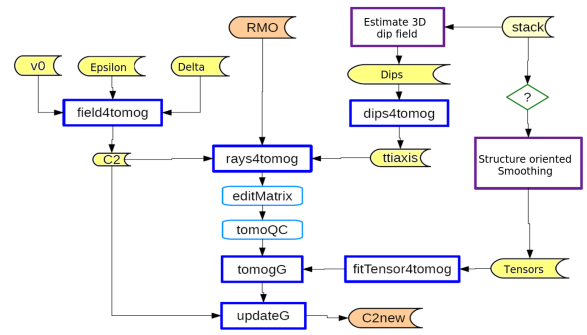
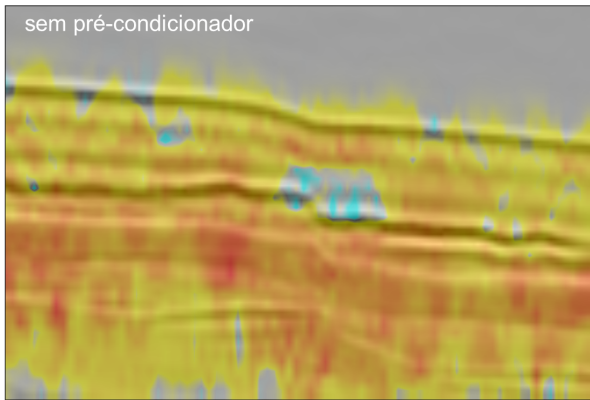


Figure 2: Flowchat for structure-guided anisotropic 3D tomography.

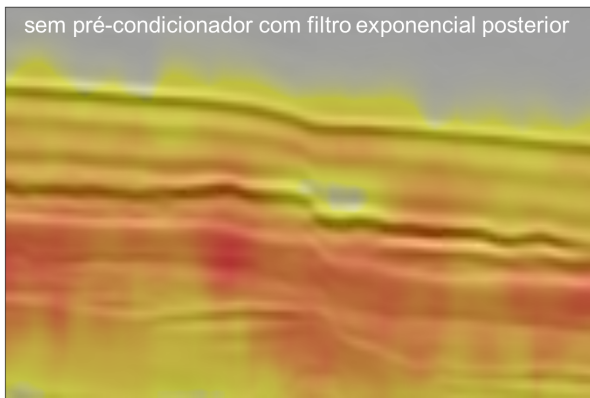
Field data applications

Initially we present field data tomography results to stress the importance of the model preconditioning in our methodology. Figures 3-6 present, in a single color scale, the model updates using four types preconditioning by model reparameterization overlaid by the corresponding migrated image. All the remaining parameters indicated in the flowchart in Figure 2 remain the same. We claim that the fault in the middle of this section present higher definition in Figure 6, also the velocity model update is more conformable to the seismic image. This feature of structure-guided tomography can be very important for seismic interpretation.



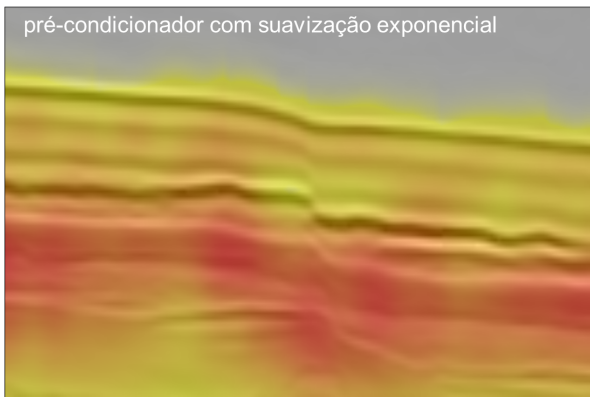
8 iterações LSMR

Figura 3: Model update without preconditioning overlaid to the corresponding migrated image.



8 iterações LSMR

Figura 4: Model update without preconditioning and using exponential filter overlaid with the corresponding migrated image.



8 iterações LSMR

Figura 5: Model update with preconditioning by exponential smoothing overlaid with the corresponding migrated image.



8 iterações LSMR

Figura 6: Model update with preconditioning by structural smoothing overlaid with the corresponding migrated image.

Our next application of the structure-guided tomography to a field dataset presents a case study where two implementations of tomography produced noticeable differences in the estimated velocity models and the resulting 3D seismic image. The baseline result is an VTI velocity model produced by a service company after five iterations of a 3D anisotropic tomography. Figure 8 shows a selected section extracted from the 3D model estimated by VTI tomography overlaid with the corresponding migrated image. The interpreter was not satisfied with the results and suggested further investigation for reducing the RMO through isotropic iterations. In order to evaluate the interpreter conjecture we used the workflow for 3D anisotropic structure-oriented tomography, as presented in the methodology section. We performed two iterations of structure-guided 3D isotropic tomography. The initial model was the vertical velocity produced by the VTI tomography. For the first iteration we used a more rigorous quality control and constrained the maximum velocity update to 25m/s and a grid of 150 m×150 m×25 m. For the second iteration the quality control was relaxed and the maximum velocity update was set to 300m/s and used refined grid 50 m×50 m×10 m. Figure 7 present a CIP gather after each iteration. One can notice the improvement in the flatness of the CIP produced by the model update in our second iteration over the whole depth range, which corroborates the interpreter hypothesis for this area.

Figures and show, respectively, the stacked migrated section for the original VTI model and the isotropic model after two iterations of structure-guided tomography overlaid with the corresponding velocity model. The isotropic model improved image focusing all over this section. The isotropic velocity model, structurally conformable, was more consistent with this dataset than the initial VTI model.

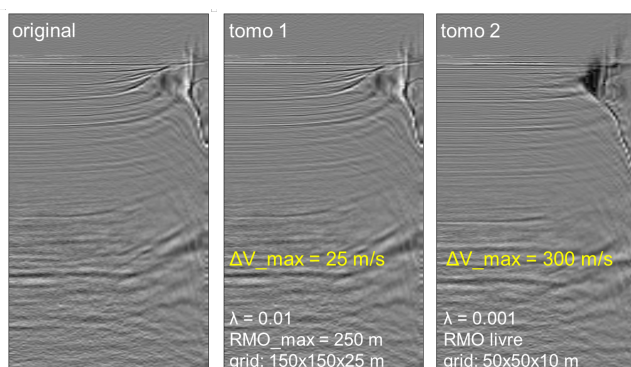


Figura 7: CIP gathers after two tomography iterations.

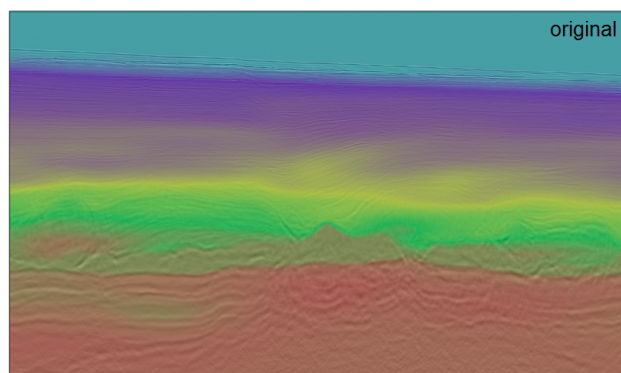


Figura 8: Vertical velocity model derived from VTI tomography overlaid with the migrated image.

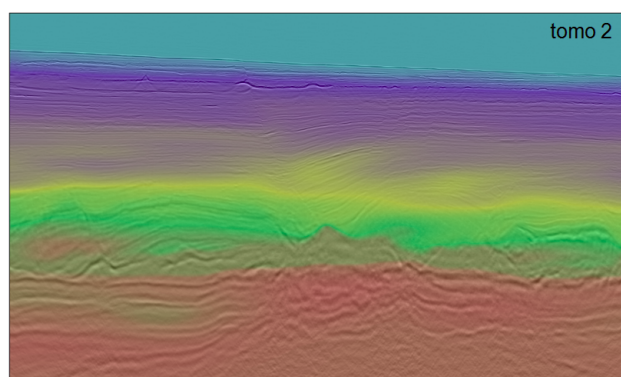


Figura 9: Isotropic velocity model derived structure-guided tomography overlaid with the migrated image.

Discussion

Our implementation of structure-guided tomography rely on dense event picking and interactive QC, a robust strategy to extract structural dip information and conditioning of the diffusivity tensor field and, preconditioning using the smoothing equation proposed by Hale (2009). Though the preconditioning at each iteration of model update requires the numerical solution of a differential equation, our numerical experiments show that it reduces significantly the number of iteration required for the convergence of the linear system solver. Moreover, this preconditioning strategy produced better results enforcing structural information on the velocity updates than alternative, computationally less expensive, filtering and smoothing operators. Another feature that was important for applications to field data sets is the model representation,

using B-splines of variable order and nonuniform meshes allows the implementation of multi-scale iterations.

We presented a successful application of structure-guided 3D tomography to improve seismic imaging and contribute to the interpretation in a field dataset offshore southeast Brazil. This case study illustrates how structure-guided isotropic iterations can fit large offset data with a structure conformable velocity model. The multi-scale strategy was instrumental to improve the resolution of the model updates. The final velocity model produced flatter CIP gathers at all depth and offset range and, significantly improved the focusing of reflection events in the final stacked migrated image. Last but not least, this result shows once again that facing ambiguity in seismic interpretation requires, besides better tools to enforce geological constraints in velocity model building, a close collaboration with the interpretation group.

Acknowledgements

We would like to acknowledge PETROBRAS for allowing the publication of this work and also all the colleagues of the exploration team.

Referências

- Bakulin, A., M. Woodward, D. Nichols, K. Osypov, and O. Zdraveva, 2010, Localized anisotropic tomography with well information in vti media: *GEOPHYSICS*, **75**, D37–D45.
- Barbosa, B., J. Costa, E. Gomes, and J. Schleicher, 2008, Resolution analysis for stereotomography in media with elliptic and anelliptic anisotropy: *GEOPHYSICS*, **73**, R49–R58.
- Clapp, R. G., B. L. Biondi, and J. F. Claerbout, 2004, Incorporating geologic information into reflection tomography: *Geophysics*, **69**, 533–546.
- Costa, J. C., F. J. da Silva, E. N. Gomes, J. Schleicher, L. A. Melo, and D. Amazonas, 2008, Regularization in slope tomography: *Geophysics*, **73**, VE39–VE47.
- De Boor, C., C. De Boor, E.-U. Mathématicien, C. De Boor, and C. De Boor, 1978, *A practical guide to splines*: springer-verlag New York, **27**.
- Fehmers, G. C., and C. F. Höcker, 2003, Fast structural interpretation with structure-oriented filtering: *Geophysics*, **68**, 1286–1293.
- Fong, D. C.-L., and M. Saunders, 2011, Lsmr: An iterative algorithm for sparse least-squares problems: *SIAM Journal on Scientific Computing*, **33**, 2950–2971.
- Golub, G. H., and C. F. Van Loan, 2012, *Matrix computations*: JHU press, **3**.
- Guo, Z., H. Dong, and Å. Kristensen, 2017, Image-guided regularization of marine electromagnetic inversion: *Geophysics*, **82**, E221–E232.
- Hale, D., 2009, *Structure-oriented smoothing and semblance*: CWP report, **635**, 261–270.
- Harlan, W. S., 1995, *Regularization by model reparameterization*: Citeseer.
- Li, V., A. Guitton, I. Tsvankin, and T. Alkhalifah, 2018, Image-guided wavefield tomography for vti media, *in* SEG Technical Program Expanded Abstracts 2018: Society of Exploration Geophysicists, 5183–5187.
- Ma, Y., D. Hale, B. Gong, and Z. Meng, 2012, Image-guided sparse-model full waveform inversion: *Geophysics*, **77**, R189–R198.
- Piegl, L., and W. Tiller, 2012, *The nurbs book*: Springer

- Science & Business Media.
- Schoenberg, M. A., and M. V. de Hoop, 2000, Approximate dispersion relations for qp-qsv-waves in transversely isotropic media: *GEOPHYSICS*, **65**, 919–933.
- Shank, R., S. Chattopadhyay, G. Rodriguez, T. Eshete, G. Hilburn, Y. He, and C. Vanschuyver, 2017, High-resolution image-guided tomography and q tomography solution for improved depth imaging for an obc survey, *in* SEG Technical Program Expanded Abstracts 2017: Society of Exploration Geophysicists, 5666–5670.
- Thomsen, L., 1986, Weak elastic anisotropy: *GEOPHYSICS*, **51**, 1954–1966.
- Wang, X., and I. Tsvankin, 2013, Ray-based gridded tomography for tilted transversely isotropic media: *GEOPHYSICS*, **78**, C11–C23.
- Woodward, M. J., D. Nichols, O. Zdraveva, P. Whitfield, and T. Johns, 2008, A decade of tomography: *GEOPHYSICS*, **73**, VE5–VE11.
- Zhou, C., J. Jiao, S. Lin, J. Sherwood, and S. Brandsberg-Dahl, 2011, Multiparameter joint tomography for tti model building: *GEOPHYSICS*, **76**, WB183–WB190.
- Zhou, J., A. Revil, and A. Jardani, 2016, Stochastic structure-constrained image-guided inversion of geophysical data: *Geophysics*, **81**, E89–E101.